Toward Direct Numerical Simulation of Reacting Fluidized Beds

M. Uhlmann, A. Pinelli, P. García-Ybarra*
Department of Fossil Fuels
CIEMAT
Av. Complutense 22, 28040 Madrid, Spain

Abstract
Nowadays, the most used techniques to design dense gas-solid flow reactors rely upon numerical predictions obtained from hydrodynamic models, usually derived through some averaging processes of the complete conservation equations. The averaging process leads to unknown correlation terms that need further modeling for the final closure of the equations. Many of these terms represent complex interactions between phases and are usually modeled through semi-empirical relations. Direct Numerical Simulation (DNS) of idealized situations can help in grasping the basic mechanisms governing these systems, therefore fostering the development of improved models.

Introduction

Dense multiphase flow reactors are part of many energy conversion and chemical catalytic units. In particular, many processes related with coal utilization involve handling of coal particles, their pneumatic transport, and their reactions in fluidized beds. One of the major factors limiting our ability to simulate these processes is the hydrodynamics encountered in them. A major issue that contributes to this limitation is the lack of good and computationally expedient models for frictional and hydrodynamic interactions between particles. This issue is of central importance in all mathematical models based on the treatment of gas-solid flows seen as fluid systems of two interpenetrating continua. In this framework, the governing equation for the two-phase flow may be obtained through a formal averaging procedure carried out on the complete set of conservation equations, *e.g*., the Navier-Stokes equations and the dynamical equations describing particle trajectories, coupled *via* the no-slip condition on the particle surface. Averaging formalisms include both the space average methods [1] and the ensemble averaging ones [2]. Independently of the employed mathematical technique, the obtained set of averaged conservation equations include a number of new correlation terms that keep into account the exchange of momentum and energy between phases taking place at microscopic level (*i.e*., unresolved scale) [1-2]. The situation becomes even more critical when reacting species need to be considered. In this case gasification reactions take place on the surface of fuel particles that will keep consuming as the reaction proceeds. In theory, under the computational point of view, one may follow two different routes. In the first one (DNS), the conservation equations are used to solve the gas phase using the proper physical boundary conditions at the surface of each particle, while following the particle evolution, *i.e*., their trajectories and volumetric changes (consumption), according to the action of the surrounding gas species. Of course, due to computer memory and power limits, such an approach can only be applied to model problems including relatively few particles (*e.g*., 10^3-10^4 particles) confined within a computational domain large enough to accommodate the typical meso-scale employed to average the original basic set of conservation equations. The second route focuses upon the meso-scale averaged equations that model the gas-solid system as a multiphase flow of interpenetrating continua. In this approach the micro-scale details are modeled while the meso-scale behavior is directly computed. This second way of dealing with the problem offers the possibility of simulating a full-scale reactor but, at the actual state of affairs, relies upon certain *a-priori* assumptions and empirical closure relationships [3]. Any improvement of multiphase descriptions of eventually reacting fluid-solid mixtures will be only achieved by a deeper understanding of the micro-scale physical mechanisms and by a systematic testing of the actual models *via a-posteriori* comparison with data obtained through detailed experiments or DNS. This paper presents the general framework and some preliminary results of an undergoing project at Ciemat to tackle the Direct Numerical Simulation of reacting fluidized beds. Specifically, the first part of the present contribution will focus upon the numerical algorithm

* Corresponding author: pg.ybarra@ciemat.es
Associated Web site: http://www.ciemat.es/
Proceedings of the European Combustion Meeting 2003

that has been selected for the simulation of non-reacting gas-solid particle systems. Some preliminary results will also be included to demonstrate the viability of the proposed numerical method. The second part will introduce the extension of the formulation to reacting systems. In particular, the case of gasification processes in fluidized bed will be considered and discussed.

Specific Objectives

The first part of the study focused on the development of an efficient algorithm able to deal with dense particulate flows. The basic requirement of the algorithm was concerned with its capability of computing the forces and the torques exerted by the gas flow on each individual rigid, spherical particle while imposing the impermeability and the no-slip condition on each particle. High computational efficiency and easiness of parallel implementation were also considered as primary issues. When the domain boundaries are complex and move in time, as in the present case, any attempt of relying upon an adapted mesh would result in an extremely heavy overhead cost due to the necessity of re-meshing the domain at each time step. Moreover, unstructured grids and non-cartesian grid systems are inherently computationally inefficient, as compared to cartesian ones, due to the unavailability of fast direct methods for the solution of the elliptic kernels arising in all the time discrete formulations of the unsteady incompressible Navier Stokes equations. In the last decade a series of numerical techniques have been proposed to extend the possibility of cartesian finite difference methods to cope with complex geometries. The common feature of all these "fictitious domain methods" concerns the way of dealing with complex boundaries. Here the boundary values to be specified on a complex geometrical shape are not explicitly accounted for by the computational grid but rather imposed implicitly by adding extra volume forces to the momentum equation of the Navier Stokes equations near fluid-solid interfaces. As a consequence, the mesh does not need to be adapted to the presence of moving solid bodies. The key point of all this methods is the way they formulate the external body forces. In the direct forcing method [4] the boundary conditions are directly imposed in the discrete operators using opportune interpolation polynomial to transfer the value from the real geometry to the grid nodes. The method proposed in [5] resorts to an explicit formulation of the non-slip condition, performing an explicit tentative step to obtain the body force distribution to be applied to restore the proper boundary values. The method proposed by Pan *et al*. and Patankar [6-7] relies upon the use of distributed Lagrangian multipliers to enforce rigidity and zero deformation rate in the solid regions. Finally, in the "immersed boundary method" [8] singular constraint forces are formulated at the solid-fluid interface by means of virtual springs and dampers. We examined almost all the mentioned methods. Implementation issues and critical reviews on the behavior of the different algorithms when dealing with solid particles in gas flows can be found at [9]. From now on, we will just focus on the "immersed boundary method". The unsteady Navier-Stokes equations, governing the fluid phase, have been discretized with a finite-difference, Runge-Kutta projection step algorithm:

$$\frac{\mathbf{u}^{*}-\mathbf{u}^{k-1}}{\Delta t} = -g_k\left[(\mathbf{u}\cdot\nabla)\mathbf{u}\right]^{k-1} - z_k\left[(\mathbf{u}\cdot\nabla)\mathbf{u}\right]^{k-2} - 2a_k\nabla p^{k-1} + a_k n\,\nabla^2\left(\mathbf{u}^{*}+\mathbf{u}^{k-1}\right) \quad (1)$$

$$\nabla^2 f^k = \frac{\nabla\cdot\mathbf{u}^{*}}{2a_k\Delta t} \quad (2)$$

$$\mathbf{u}^k = \mathbf{u}^{*} - 2a_k\Delta t\nabla f^k \quad (3)$$

$$p^k = p^{k-1} + f^k - a_k\Delta t n\,\nabla^2 f^k \quad (4)$$

$$a_k = \left\{\tfrac{4}{15},\tfrac{1}{15},\tfrac{1}{6}\right\},\ g_k = \left\{\tfrac{8}{15},\tfrac{5}{15},\tfrac{3}{4}\right\},\ z_k = \left\{0,-\tfrac{17}{60},-\tfrac{5}{12}\right\}$$

Where k = 1, 2, 3 is the Runge-Kutta step counter. The given coefficients provide for second order accuracy both in pressure and in gas velocity [9]. Some caution must be taken when applying the same time advancement scheme to the solid particles embedded within the gas flow. In particular, when considering rigid, impermeable particles submerged within an incompressible flow, the most convenient way of expressing the equations for the particle motion reads like:

$$V_c\left(r_c - r_f\right)\dot{\mathbf{u}}_c = -r_f\int_S \mathbf{f}\,\mathrm{d}V + \mathbf{G}_c \quad (5)$$

$$I_c\mathbf{w}_c = -r_f\int_S(\mathbf{r}\times\mathbf{f})\,\mathrm{d}V + r_f\frac{\mathrm{d}}{\mathrm{d}t}\int_S(\mathbf{r}\times\mathbf{u})\,\mathrm{d}V \quad (6)$$

Where V_c is the particle volume, r_c and r_f are, respectively, the solid and the fluid densities, I_c is the particle moment of inertia, $\mathbf{u}_c$ and $\mathbf{w}_c$ are, respectively the linear and the angular velocities of the center of mass, and $\mathbf{f}$ is the force exerted by the fluid on the particle surface. A time scheme, consistent (*i.e*., same truncation error) with the three stages given for the gas phase, reads as follows:

$$\frac{\mathbf{u}_c^k-\mathbf{u}_c^{k-1}}{\Delta t} = \frac{r_f}{V_c(r_c-r_f)}\left(-g_k\int_S\mathbf{f}^k\,\mathrm{d}V - z_k\int_S\mathbf{f}^k\,\mathrm{d}V\right) \quad (7)$$

$$\frac{\mathbf{x}_c^k-\mathbf{x}_c^{k-1}}{\Delta t} = a_k\left(\mathbf{u}_c^k+\mathbf{u}_c^{k-1}\right) \quad (8)$$

$$\frac{\mathbf{w}_c^k-\mathbf{w}_c^{k-1}}{\Delta t} = \frac{r_f}{p\,r_c^4\left(r_c-r_f\right)/2}\left[-g_k\int_S(\mathbf{r}\times\mathbf{f})^k\,\mathrm{d}V - z_k\int_S(\mathbf{r}\times\mathbf{f})^k\,\mathrm{d}V\right] \quad (9)$$

$$\frac{\mathbf{q}_c^k-\mathbf{q}_c^{k-1}}{\Delta t} = a_k\left(\mathbf{w}_c^k+\mathbf{w}_c^{k-1}\right) \quad (10)$$

being, $\mathbf{x}_c$ the position of the center of mass, and $\mathbf{q}_c$ the orientation with respect to a fixed reference system mounted on the particle. The fluid equations are

discretized in space using second order finite difference formulae with the variable collocated in a staggered fashion.

Immersed Boundary Method

The immersed boundary method has initially been developed by Peskin and co-workers for the simulation of the flow in the human heart and then extended to a variety of related problems [8]. The specific aim of the method was to allow for the numerical representation of singular forces at Lagrangian locations within an Eulerian solver. While in the original problem of immersed fibers or membranes (heart valves), the expression for the singular forces is known, in the present case of immersed rigid bodies, it requires an *ad hoc* introduction of adequate springs and dampers [10]. To explain the method, first, we introduce the curvilinear coordinate s (with $0 \le s \le L_b$) which runs along the fluid-solid interface of the immersed body under consideration; $\mathbf{X}(s,t)$ defines the position of the interface in time. The body force to be applied to the Navier-Stokes equations (*i.e.*, to the right hand side of equation 1) is then expressed as follows:

$$\mathbf{F}(s,t) = k\left[\mathbf{X}^{(d)}(s,t) - \mathbf{X}(s,t)\right] + 2g\,\partial_t\left[\mathbf{X}^{(d)}(s,t) - \mathbf{X}(s,t)\right] \qquad (11)$$

$$\mathbf{f}(s,t) = \int_0^{L_b} \mathbf{F}(s,t)\,d\left[\mathbf{x} - \mathbf{X}(s,t)\right]\mathrm{d}s$$

The singular force $\mathbf{F}(s,t)$ which acts at the Lagrangian locations $\mathbf{X}(s,t)$ is given by the force obtained as if springs with stiffness k and dampers with damping constants g would be attached between the present location $\mathbf{X}(s,t)$ of the interface and its "desired" location $\mathbf{X}^{(d)}(s,t)$. By "desired location" we mean the material locations given by the known position of the body's center and its angle of rotation together with the rigidity constraint; the center can be stationary, undergo a forced or a free movement. This formulation of the forces serves to maintain the solid close to its desired location against the action of the hydrodynamic forces. In practice, we have neglected the damping part of the forces altogether ($g = 0$); the authors in [11] did retain it. As indicated in equation (11), the Lagrangian force is transferred to the Eulerian representation, $\mathbf{f}(x,t)$, by means of a convolution which involves the Dirac function of the difference between the Eulerian and the Lagrangian position vectors ("spreading"). Finally, the Lagrangian locations need to be computed from the fluid velocity at the respective locations, $\mathbf{U}(s,t)$, which in turn are obtained by transferring the Eulerian velocities to the Langrangian points ("interpolation"):

$$\mathbf{U}(s,t) = \int_\Omega \mathbf{u}(\mathbf{x},t)\,d\left[\mathbf{x} - \mathbf{X}(s,t)\right]\mathrm{d}\mathbf{x} \qquad (12)$$

$$\partial_t \mathbf{X}(s,t) = \mathbf{U}(s,t) \qquad (13)$$

In order to introduce a discretized version of the algorithm we define a grid of equidistant intervals along the curvilinear coordinate s: the set $s_k = (k-1)\Delta s$, $k = 1,\ldots,n$, with $\Delta s \equiv L_b/\,n$ (L_b being the length of the boundary and n the number of nodes distributed on it, in practice $\Delta s \approx \Delta x$). The spatial location of these discrete knots $\mathbf{X}(s_k)$ are usually termed as "Lagrangian marker points". For simplicity, we will suppose, from here on, that the underlying Cartesian grid is such that $\Delta x = \Delta y$. The Dirac delta functions appearing in (12) and (13) need to be regularized to achieve a discrete approximation [8]:

$$d_h(\mathbf{x}) = d_h\left(\frac{x}{\Delta x}\right)\cdot d_h\left(\frac{y}{\Delta y}\right)\frac{1}{\Delta x \Delta y} \qquad (14)$$

$$d_h(r) = \begin{cases} \frac{1}{3}\left(3 - 2|r| + \sqrt{1 + 4|r| - 4r^2}\right) & |r| \le 1 \\ \frac{1}{3}\left(5 - 2|r| - \sqrt{-7 + 12|r| - 4r^2}\right) & 1 \le |r| \le 2 \end{cases}$$

$$\text{otherwise, } d_h(r) = 0 \qquad (15)$$

Important properties of this choice are: *i*) compact support (with a radius of $2\Delta x$) which leads to computational efficiency in performing the "spreading" and "interpolation" operations between Eulerian and Lagrangian grids; *ii*) continuity of the function $d_h(r)$ for real arguments r which allows for smooth transition of moving Lagrangian objects over the fixed grid; *iii*) second-order accurate interpolation for "smooth" fields at solid boundaries (when derivatives of velocity and pressure have a jump, the method leads to first-order spatial accuracy). In the following, we will consider an explicit coupling between solid and fluid phases, meaning that the formulation of the volume forces is explicit (the viscous terms are treated implicitly). Lai and Peskin [10] use a second-order time and space accurate predictor-corrector scheme. Here, we incorporate the immersed boundary method into the aforementioned three-step Runge-Kutta method. The resulting algorithm reads, at each R-K stage as:

$$\mathbf{F}^k(s_i) = k\left[\mathbf{X}^{(d)}(s_i,t) - \mathbf{X}^{k-1}(s_i)\right] + 2g\left[\mathbf{U}^{(d)}(s_i,t) - \mathbf{U}^{k-1}(s_i)\right] \qquad (16)$$

$$\mathbf{f}^k(\mathbf{x}) = \sum_i \mathbf{F}^k(s_i)\,d_h\left[\mathbf{x} - \mathbf{X}^{k-1}(s_i)\right]\Delta s \qquad (17)$$

$$\frac{\mathbf{u}^* - \mathbf{u}^{k-1}}{\Delta t} = a_k n\,\nabla^2\left(\mathbf{u}^{k-1} + \mathbf{u}^*\right) - 2a_k \nabla p^{k-1} - g_k\left[(\mathbf{u}\cdot\nabla)\mathbf{u}\right]^{k-1} - z_k\left[(\mathbf{u}\cdot\nabla)\mathbf{u}\right]^{k-2} + g_k \mathbf{f}^k + z_k \mathbf{f}^{k-1} \qquad (18)$$

$$\nabla^2 f^k = \frac{\nabla\cdot\mathbf{u}^*}{2a_k\Delta t} \qquad (19)$$

$$\mathbf{u}^k = \mathbf{u}^* - 2a_k\Delta t \nabla f^k \qquad (20)$$

$$p^k = p^{k-1} + f^k - a_k \Delta t n \, \nabla^2 f^k \quad (21)$$

$$\mathbf{U}^k(s_i) = \sum_{i,j} \mathbf{u}^k(\mathbf{x}_{i,j}) d_h\left[\mathbf{x}_{i,j} - \mathbf{X}^{k-1}(s_i)\right] \Delta x \Delta y \quad (22)$$

$$\mathbf{X}^k(s_i) = \mathbf{X}^{k-1}(s_i) + a_k \Delta t \left[\mathbf{U}^k(s_i) + \mathbf{U}^{k-1}(s_i)\right] \quad (23)$$

Note that the volume forces in (18) are integrated with the same scheme as the non-linear terms in the predictor step in order to guarantee second-order overall consistency (for smooth fields); for the same reason, the position of the marker points in (23) is integrated with the same Crank-Nicholson-type scheme as the viscous terms. This formulation has implications for the determination of the total volume force added to the fluid during a full time step. Furthermore, it should be noted that the time-level of the desired locations in (16) was not exactly specified for the time being. Here, we will use the prescribed locations at the end of the time step, i.e., $\mathbf{X}^{(d)}(s_i, t + \Delta t)$, throughout the Runge-Kutta sub-steps; in the case of freely-moving particles, the two-way coupling is described in details in [9]. The discretization of the spatial operators $\nabla, \nabla\cdot, \nabla^2$ is carried out as usual in the framework of a staggered finite difference formulation. The main disadvantage of the immersed boundary method is that an additional free parameter, the stiffness k, is introduced. Its value needs to be selected manually such that *i*) the solid body is not appreciably deformed during the computation, and *ii*) the allowed time step restriction is not too severe. In reference [10], a rough estimate for the time step is given as $\Delta t \sim (\Delta x/k)^{1/2}$, which shows that considerations *i*) and *ii*) are opposed as far as the value of k is concerned. In practice, however, we were able to find a reasonable compromise.

Simulation of Reactive Beds

Consideration of chemical reactions taking place in fluidized beds significantly increases the complexity of the study. Restricting our discussion to combustion and gasification reactors, the large heat capacity of the solid bed particles compared to the surrounding gas and the strong mixing that prevails in the bed allow to undertake the following simplifying description. Let us assume that local thermal and chemical equilibrium hold over the meso-scale. Accordingly, temperature and chemical species concentrations will undergo slow variations, for instance, along the reactor radius R, in most of the reactor bulk. Nevertheless, sharp transitions have necessarily to occur in the vicinity of the fuel particles and at the interface separating the gas-solid disperse phase from the uprising air streams/bubbles. In these zones transitional boundary layers appear to accommodate the equilibrium concentration values to those dictated by the locally predominant chemical reactions. The relative thickness of these layers, with respect to R, is of the order of the inverse of the square root of the local Damkhöler number, defined as the ratio of the mixing time to the chemical time. At the relatively high temperatures found in the reactor, this ratio takes on very large values thus leading to very thin non-equilibrium layers. On the surface of each fuel particle, gasification reactions take place, which dictate the local values of the species concentrations, both the consumed gasifying species (steam, CO_2…), and the produced gaseous fuels (H_2, CO…). Similarly at the separation boundary between the oxygen-lean disperse phase zone and the oxygen-rich blowing air regions, oxidation (combustion) reactions occur in a diffusion flame sheet, along the reactor, until one of the reactants (fuel in combustors or oxygen in gasifiers) is depleted. Thus, in the meso-scale description, solid fuel particles appear as volumetric sinks (resp., sources) of gasifying (resp., gaseous fuel) species whereas the air stream – disperse phase boundaries are surface sources (resp., sinks) of gasifying species (resp., fuel and oxygen). The results of this analysis at the mesoscopic scale provide the far-field values for the species concentration profiles in the microscopic description of the thin reactive layers.

In particular, regarding the micro-scale DNS computation, gasification reactions strongly affect the values of the particle drag/lift coefficients. Depending on the local chemical equilibrium values, the gasification rate of each fuel particle should relate to its shrink/swelling rate and leads to a variable particle radius. Even more, particle gasification deliver a net radially outgoing gas flow significantly reducing the particle-gas friction.

Results and Discussion

An important first step in the direction of computing particulate flows is the simulation of flow around a stationary cylinder, which demonstrates the capability of the method to capture the hydrodynamic forces acting upon the solid body with reasonable precision. To this end we considered a cylinder with diameter D located at the origin. The chosen domain size ($27D \times 27D$) corresponds to the one of [10] and has to be considered marginal as far as the influence due to the boundaries (particularly the confinement of the flow at the lateral boundaries) is concerned. We have performed computations with three Reynolds numbers based upon cylinder diameter and free-stream velocity: Re = 1, 10, 100. The grid consisted of 512×512 uniformly distributed nodes, i.e., the coarser grid of [9]. The stiffness coefficient k was set to 48000 and the cylinder perimeter was discretized using 50 knots. With these values the maximum deviation from the desired geometry was measured to be $0.0002D$. The initial field was set to uniform, unidirectional flow. For Re =1 and 10 the flow reaches a steady state exhibiting a symmetric wake. In the case of Re = 100, an

alternating vortex shedding behavior is obtained. In the unsteady case the reference time is set to $t_{ref} = D/(2u_\infty)$ and the Strouhal number is $St = (f_n D)/u_\infty$ being f_n the shedding frequency. The integral quantities of interest are the drag coefficient and lift one. The following table shows the present results versus reference values (+ Oseen´s formula;× experimental data; * computations [10]).

Present Results

Re_D	C_D	C_L	St
1	14.0643	-	-
10	3.14318	-	-
100	1.39423	0.35573	0.174

Reference Results

Re_D	C_D	C_L	St
1	+ 12.56		-
10	× 3.0		-
100	* 1.33	* 0.33	* 0.165

It can be seen that the dimensionless coefficients are reasonably well captured for both the steady and the unsteady cases. The correspondence with the reference data could be further improved by enlarging the computational domain.

The next step to test the effectiveness of the method to cope with moving particles was to let the solid object perform a prescribed (externally forced) movement. To this end, we added a periodical vertical movement of the cylinder axis:

$$y_c(t) = A_y \cos(2p\ f_f t)$$
$$v_c(t) = 2p\ f_f A_y \sin(2p\ f_f t)$$

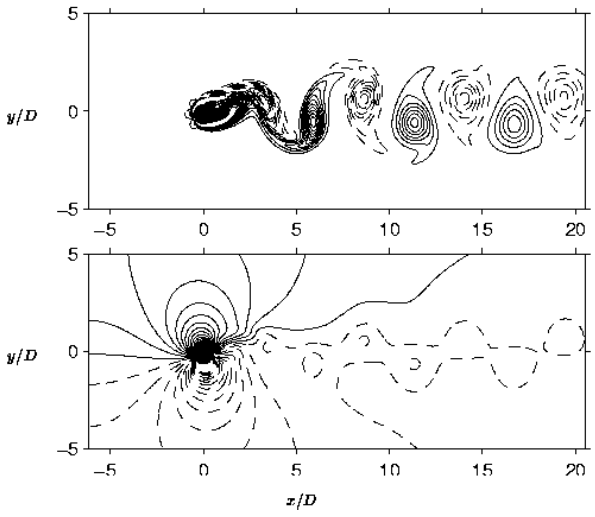

Fig. 1. Instantaneous vorticity (top) and pressure (bottom) fields for the oscillating cylinder in cross flow (Re = 100)

The amplitude of the motion was chosen to be $A_y = D/4$, and the frequency fixed to the natural shedding frequency at Re =100 (*i.e.*, $f_f \approx 0.166u_\infty/D$, steady cylinder). The horizontal position is fixed and no angular movement is allowed. This case, investigated in [12], corresponds to a translationally oscillating cylinder in a cross-flow. Figure 1 shows an instantaneous vorticity and pressure field at Re = 100. Quantitative comparisons with the literature data [12] show a quite acceptable agreement thus indicating that the present method is indeed a potential candidate for the simulation of particulate flows.

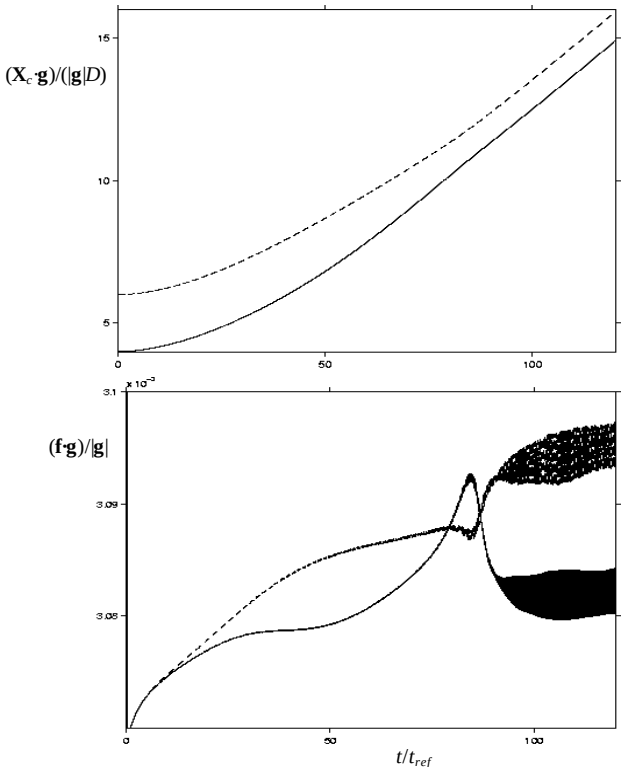

Fig. 2. Particles centers locations (top) and hydrodynamic force (bottom) in gravity direction: --- leading; — trailing.

As a further check of the suitability of the method to cope with fluidized beds, we considered the case of two or more particles accelerating from rest due to gravity within a quiescent fluid. Here we will focus only upon the case of two particles, one leading the other by twice the diameter, since other authors have considered it as well [13-14]. Much more complex conditions have been considered and analyzed too [9]. For the mentioned case of two free falling identical particles, the domain was set to 8R long (in the gravity direction), 2R large. The initial position of particle 1 was at (0.8R,1.001R), while the one of particle 2 was at (1.2R,1R), *i.e.*, with a slight offset in the gravity free direction to promote the "tumbling" of the particles. The mesh size and the time step were fixed to 0.005 and 0.0002 respectively. k was fixed to 1.25×10^5 and the number of Lagrangian markers on each body was 125. The physical parameters affecting the simulation (MKS) were: n = 0.001 (fluid kinematic viscosity), $|\mathbf{g}|$ = 9.81, D = 0.1, r_p = 1.01, r_f = 1.00. The corresponding

non-dimensional numbers are: $Re = D\,u_{ref}/n = 22.98$, $Fr = u_{ref}/(|\mathbf{g}|\,D)^{1/2} = 0.082$ [here u_{ref} is the terminal velocity: $u_{ref}=(|\mathbf{g}|\,D)^{1/2}$] and the density ratio. Thus, the non-dimensional time is $t_{ref} = (D/|\mathbf{g}|)^{1/2}$. Figure 2 shows the position of the two particles during 120 t/t_{ref}. This is the duration up to the initial particle interaction, *i.e*., drafting and kissing but no tumbling yet due to the limited container size. At larger times, the vicinity of the "bottom" of the container was interfering with the interaction. The results of [13] and data provided by T.W. Pan (private communication) for particle positions correspond closely and are omitted in the figure. Also shown are the hydro-dynamical forces. Initial oscillations on the time scale of the virtual springs are visible. This is why the damping forces are necessary. At later stages, *i.e*., for $t/t_{ref} > 80$ the forces are oscillating with a moderate amplitude and on a short time scale. This effect is due to the two particles coming into contact (getting so close to each other that probably the flow field in between the particles cannot be adequately resolved anymore). This brings us to the question of the eventual necessity of inter-particle repulsion forces [14].

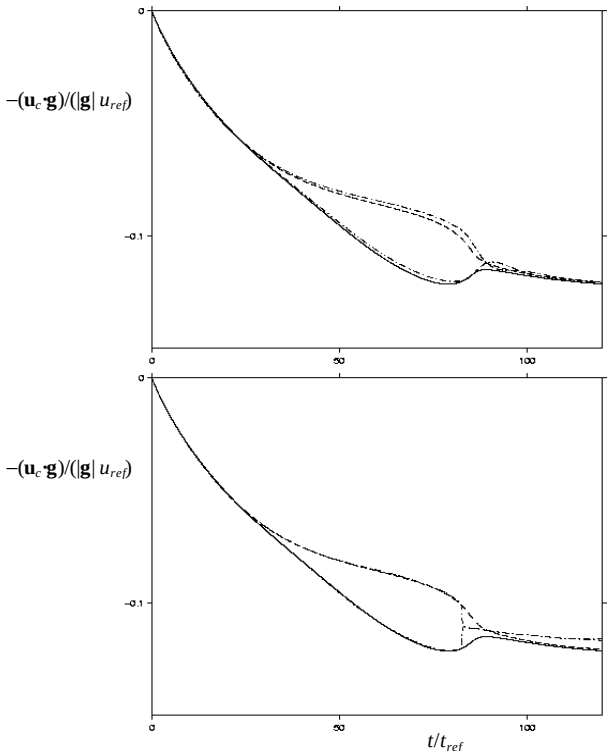

Fig. 3. Center of mass velocity in gravity direction: --- leading; — trailing. (a) comparison with [13], (b) with Pan data (both in chain-dotted lines).

Finally, Figure (3) shows the velocity in the direction of the gravitational vector. We have plotted our present results against those of [13] and those of T.W. Pan (private communication). The agreement between all three methods is excellent up to $t/t_{ref} \approx 80$ Afterwards, the results of [13] still match the present ones closely while in Pan's simulation the two particles "synchronize" their velocity nearly instantaneously when coming into contact. It should be noted that in Pan's computation, an explicit repulsion force is introduced while the other two methods are free of such treatment.

Conclusions

DNS is being used as a tool to get a deeper understanding of the dissipative phenomena playing at the micro-scale (particle-particle interaction) in fluidized bed reactors. Nevertheless, to reach the final objective, *i.e*., DNS of reacting gas particle systems, much work needs to be carried out yet. The main issues to be dealt subsequently should be: particle collisions (solid-solid ones), alleviation of the actual time step restriction; three-dimensional extension and implementation of the proposed reactive bed model.

Acknowledgements

The Spanish Ministry of Science and Technology has supported this work through grant number DPI2002-04550-C07-04

References

[1] R. Jackson, *The Dynamics of Fluidized Particles*, Cambridge Monographs on Mechanics, Cambridge University Press, 2000.

[2] D. Z. Zhang, A. Prosperetti, *Int. J. Multiphase Flow.* **23** (1997) 425.

[3] S. Sundaresan, *AIChE Journal*.**46**, (2000) 1102.

[4] E. A. Fadlun, R. Verzicco, P. Orlandi, J. M. Yusof, *J. Comput. Physics*. **163** (2000) 35.

[5] J. Kim, D. Kim, H. Choi, *J. Comput. Physics*. **171** (2001) 132.

[6] T. W. Pan, D. D. Joseph, R. Bai, R. Glowinski, V. Sarin, *J. Fluid Mech*. **451** (2002) 169.

[7] N. A. Patankar, *Center for Turbulence Research Res*. Briefs, Stanford University (2001) 185.

[8] C. S. Peskin, *Acta Numerica* (2002) 1.

[9] www.ciemat.es/sweb/comfos/personal/uhlmann/home/report.html

[10] M. C. Lai, C. S. Peskin, *J. Comput. Physics*. **160** (2000) 165.

[11] K. Hofler, S. Schwarzer, *Phys. Rev. E*, (2000)

[12] H. M. Blackburn, R.D. Henderson, *J. Fluid Mech*. **385** (1999) 255.

[13] Z. Zhang, A. Prosperetti, *J. Applied Mech*. **70** (2003) 1.

[14] N. A. Patankar et al. *Int. J. Multiphase Flow.* **24** (2000) 1509.